2015

Estimation of spruce needle-leaf chlorophyll content based on DART and PARAS canopy reflectance models

Lucia Yanez-Rausell
Wageningen University

Zbynek Malenovky
University of Wollongong, zbynek@uow.edu.au

Miina Rautiainen
University of Helsinki

Jan G. P. W Clevers
Wageningen University

Petr Lukes
University of Helsinki

See next page for additional authors

Publication Details

Yanez-Rausell, L., Malenovky, Z., Rautiainen, M., Clevers, J. G. P. W., Lukes, P., Hanus, J. & Schaepman, M. E. (2015). Estimation of spruce needle-leaf chlorophyll content based on DART and PARAS canopy reflectance models. IEEE Journal of Selected Topics in Applied Earth Observations and Remote Sensing, 8 (4), 1534-1544.

Estimation of spruce needle-leaf chlorophyll content based on DART and PARAS canopy reflectance models

Abstract
Needle-leaf chlorophyll content (Cab) of a Norway spruce stand was estimated from CHRIS-PROBA images using the canopy reflectance simulated by the PROSPECT model coupled with two canopy reflectance models: 1) discrete anisotropic radia- tive transfer model (DART); and 2) PARAS. The DART model uses a detailed description of the forest scene, whereas PARAS is based on the photon recollision probability theory and uses a simplified forest structural description. Subsequently, statisti- cally significant empirical functions between the optical indices ANCB 670 – 720 and ANMB 670 – 720 and the needle-leaf Cab content were established and then applied to CHRIS-PROBA data. The Cab estimating regressions using ANMB 670 – 720 were more robust than using ANCB 670 – 720 since the latter was more sensitive to LAI, especially in case of PARAS. Comparison between Cab esti- mates showed strong linear correlations between PARAS and DART retrievals, with a nearly perfect one-to-one fit when using ANMB 670 – 720 (slope = 1.1, offset = 11 μ g · cm – 2). Further com- parison with Cab estimated from an AISA Eagle image of the same stand showed better results for PARAS (RMSE = 2.7 μ g · cm – 2 for ANCB 670 – 720 ;RMSE = 9.5 μ g · cm – 2 for ANMB 670 – 720)than for DART (RMSE = 7.5 μ g · cm – 2 for ANCB 670 – 720 ;RMSE = 23 μ g · cm – 2 for ANMB 670 – 720). Although these results show the potential for simpler models like PARAS in estimating needle-leaf

Disciplines
Medicine and Health Sciences | Social and Behavioral Sciences

Publication Details
Yanez-Rausell, L., Malenovky, Z., Rautiainen, M., Clevers, J. G. P. W., Lukes, P., Hanus, J. & Schaepman, M. E. (2015). Estimation of spruce needle-leaf chlorophyll content based on DART and PARAS canopy reflectance models. IEEE Journal of Selected Topics in Applied Earth Observations and Remote Sensing, 8 (4), 1534-1544.

Authors
Lucia Yanez-Rausell, Zbynek Malenovky, Miina Rautiainen, Jan G. P. W Clevers, Petr Lukes, Jan Hanus, and Michael E. Schaepman

Estimation of Spruce Needle-leaf Chlorophyll Content Based on DART and PARAS Canopy Reflectance Models

Yáñez-Rausell, L., Malenovský, Z., *Member, IEEE*, Rautiainen, M., Clevers, J. G. P. W., Lukeš, P., Hanuš, J., and Schaepman, M. E., *Senior Member, IEEE*

***Abstract*—Needle-leaf chlorophyll content (Cab) of a Norway spruce stand was estimated from CHRIS-PROBA images using the canopy reflectance simulated by the PROSPECT model coupled with two canopy reflectance models DART and PARAS. The DART model uses a detailed description of the forest scene, whereas PARAS is based on the photon recollision probability theory and uses a simplified forest structural description. Subsequently, statistically significant empirical functions between the optical indices $ANCB_{670–720}$ and $ANMB_{670–720}$ and the needle-leaf Cab content were established and then applied to CHRIS-PROBA data. The Cab estimating regressions using $ANMB_{670–720}$ were more robust than using $ANCB_{670–720}$ since the latter was more sensitive to LAI, especially in case of PARAS. Comparison between Cab estimates showed strong linear correlations between PARAS and DART retrievals, with a nearly perfect one-to-one fit when using $ANMB_{670–720}$ (slope = 1.1, offset = 11 µg cm^{-2}). Further comparison with Cab estimated from an AISA Eagle image of the same stand showed better results for PARAS (RMSE = 2.7 µg cm^{-2} for $ANCB_{670-720}$; RMSE = 9.5 µg cm^{-2} for $ANMB_{670-720}$) than for DART (RMSE = 7.5 µg cm^{-2} for $ANCB_{670-720}$; RMSE = 23 µg cm^{-2} for $ANMB_{670-720}$). Although these results show the potential for simpler models like PARAS in estimating needle-leaf Cab from satellite imaging spectroscopy data, further analyses regarding parameterization of radiative transfer models are recommended.**

***Index Terms*—Chlorophyll a+b estimation, CHRIS-PROBA, coniferous forest, continuum removal, DART, needle-leaf, Norway spruce, optical indices, PARAS, PROSPECT, radiative transfer, recollision probability**

Manuscript received in March, 11th, 2014. This work was supported in part by the University of Zurich Research Priority Program on 'Global Change and Biodiversity' (URPP GCB). The work of Z. Malenovský was supported by the 'AirLIFT' discovery project of the Australian Research Council (DP140101488). The work of M. Rautiainen was financed by the Academy of Finland. Contribution of J. Hanuš from the CzechGlobe Centre was co-financed by EU funds and the State Budget of the Czech Republic (CZ.1.05/1.1.00/02.0073).

L. Yáñez-Rausell is with the Laboratory of Geo-Information Science and Remote Sensing, Wageningen University, PO BOX 47, 6700 AA Wageningen, The Netherlands (l.yanezrausell@gmail.com) and the Department of Geography, Univ. of Zurich, Winterthurerstrasse 190, CH-8057 Zurich, Switzerland (lucia.yanezrausell@geo.uzh.ch).

Z. Malenovsky is with the School of Biological Sciences, University of Wollongong, Northfields Ave, NSW 2522, Australia (zbynek.malenovsky@gmail.com).

M. Rautiainen is with University of Helsinki, Department of Forest Sciences, P.O. Box 27, FI-00014 University of Helsinki, Finland (miina.rautiainen@helsinki.fi).

J. G. P. W. Clevers is with the Laboratory of Geo-Information Science and Remote Sensing, Wageningen University, Wageningen, The Netherlands (e-mail: jan.clevers@wur.nl).

P. Lukeš is with University of Helsinki, Department of Forest Sciences, P.O. Box 27, FI-00014 University of Helsinki, Finland (petr.lukes@helsinki.fi).

J. Hanuš is with CVGZ AV ČR-CzechGlobe, Bělidla 986/4a, 603 00 Brno, Czech Republic (e-mail: hanus.j@czechglobe.cz).

M. E. Schaepman is with the Department of Geography, Univ. of Zurich, Winterthurerstrasse 190, CH-8057 Zurich, Switzerland (michael.schaepman@geo.uzh.ch).

I. Introduction

CHLOROPHYL spectral absorption in blue and red parts of the electromagnetic spectrum can be exploited by optical remote sensing (RS) to quantify the leaf chlorophyll *a* and *b* content (Cab) [1]. Established RS methods for estimating Cab are based on empirical approaches, more complex radiative transfer (RT) models, or combination of both (see reviews from [2-4]). RT methods are required especially in case of heterogeneous environments, where canopy structure plays a major role in the scattering processes [5, 6]. Coniferous forest stands represent such structurally complex environments due to the specific clumping of needle-leaves into shoots [7-9]. This produces high multiple scattering that causes decrease of reflected light in the near-infrared (NIR) region when compared to broadleaf forests [10, 11].

Some 3D RT models attempted to consider the shoot clumping and between-shoot scattering effects of the foliage inside the conifer crown. For example, in the 5-Scale model shoots are defined as the elementary foliage units, which are randomly distributed along the branch [12]. The Discrete Anisotropic Radiative Transfer model (DART; [13]) does not include direct description of shoots, but it allows creating 3D foliage clumps using turbid voxels of varying size defined by a specific leaf and twig area index, and leaf and twig angle distribution. The turbid cells are distributed in a specific pre-defined way along the branches simulated as geometrical primitives emerging from trunks (e.g. [14, 15]). Still, the scattering phase functions are computed from leaf and bark optical properties without accounting for scattering of the shoot units (see review from [16]). Despite of this

simplification, [14] showed that definition of ecologically correct tree crown architecture in DART model could result in accurate estimation of Cab even in case of a complex coniferous canopy. This approach, however, requires many input parameters and it is computationally demanding.

An alternative with a simpler parameterization of coniferous canopy structure, but taking into account the shoot-level scattering, is a physically based model named PARAS [11]. PARAS simulates the canopy bidirectional reflectance factor (BRF, for terminology see [17]) by upscaling the leaf scattering albedo (i.e., leaf reflectance plus transmittance) through a spectrally invariant parameter called the photon recollision probability (p), which is the probability with which a photon scattered by the canopy will interact again with a canopy phytoelement [18]. The PARAS model was used to investigate the effect of structural parameters on forest reflectance [19, 20], but has not been tested for estimation of Cab of forest stands yet.

The objective of this paper is to compare the performance of both canopy RT models, DART and PARAS, when employed in the estimation of coniferous needle-leaf Cab from satellite imaging spectroscopy data at about 20 m spatial resolution. By using Cab sensitive optical indices, we will evaluate how much the leaf Cab estimates retrieved using a detailed 3D structural forest description in DART differs from the ones produced using a simpler structural parameterization in PARAS. Comparable performance of both models would imply that Cab retrieval of the same accuracy can be achieved with computationally less intensive RT modelling conference.

II. Materials And Methods

A. Study area and CHRIS-PROBA satellite image data

The study area was a regularly planted Norway spruce (Picea abies /L./ Karst.) stand (an area of 11,560 m^2) at the permanent eco-physiological research site "Bílý Kříž" (Moravian-Silesian Beskydy Mountains; 18.54º E, 49.50º N, mean elevation of 894 m a.s.l.) in Czech Republic. CHRIS-PROBA (Compact High Resolution Imaging Spectrometer) satellite images [21] of the study area were acquired on 12th September 2006 in sensor mode 4, i.e. 18 channels located in the spectral region of 485 – 800 nm, with a bandwidth ranging from 5.8 to 14.9 nm, and a nadir spatial resolution of 17 m. At the time of the CHRIS-PROBA acquisition, the stand was about 29-years old with tree density of 1430 stems.ha^{-1}. The canopy cover (CC) of about 80-90% strongly reduced the influence of the forest background on the satellite data. For this study, we used a radiometrically and atmospherically corrected nadir reflectance image [22].

B. Field measurements

A set of 81 needle-leaf samples of the last three age-classes was collected from three levels of the vertical crown profile (upper ~ sun exposed (E), middle ~ transitional (T), and lower ~ shaded (S)) around the CHRIS-PROBA acquisition time. Samples were deep frozen in liquid nitrogen transferred to a laboratory and processed to quantify biophysical properties required for modelling the needle optical properties as described in [14]. The directional-hemispherical reflectance functions (DHRF) of five spruce bark samples were measured as described in [23].

Since the forest floor of the study site was mostly composed of litter (senescent needle-leaves) with occasionally spots of bare soil, the optical properties of the forest background were derived as the weighted mean of DHRF measurements of both these surfaces [23]. Weights corresponded to the surface's abundance ratio of 1/3 of bare soil and 2/3 of senescent needle-leaves (Fig. 1d).

Above and below-canopy measurements done with the LAI-2000 Plant Canopy Analyzer (Li-Cor, Inc., USA) were collected as a part of a continuous LAI monitoring carried out in two forest plots with different stand densities according to [24]. The readings from 2005 to 2007 (unpublished) were used to compute the effective leaf area index (LAI_{eff}), the canopy gap fraction (*cgf*) and the so-called "diffuse non-interceptance" (DIFN) used for the BRF simulations by the PARAS model (section II.E). The true LAI of the study site in 2006 was 7-9 (computed using 3 different approaches; Table 2 in [25]). Additional canopy structural parameters required for the 3D forest scene creation in the DART model [23] were obtained from destructive measurements of tree individuals [22, 26].

C. Needle-leaf reflectance and transmittance simulations

First, needle-leaf reflectance (R_L) and transmittance (T_L) were simulated with the PROSPECT leaf RT model (version 3) [27], adjusted for Norway spruce needles by [28]. The PROSPECT inputs for water and dry matter content were derived from 81 needle samples that were collected from 9 trees located across the elevation gradient. The structural mesophyll parameter N was retrieved for each sample from DHRF measurements as in [14]. Since the spectral region used for Cab retrievals is not significantly sensitive to the N number [28], a single average of all retrieved N values was applied. Finally, the variable of interest (Cab) was varied from 10 to 100 µg cm^{-2} with an increment of 10 µg cm^{-2}. The lowest and the highest values were set 10 µg cm^{-2} below and above the minimal and the maximal values measured at the study site from more than 300 samples analyzed between 2004 and 2007. All PROSPECT inputs and their measured standard deviations are summarized in Table I (for more details about the PROSPECT parameterization see [28] and [14]).

The nine PROSPECT simulated R_L and T_L, i.e. three needle age-classes of exposed, transitional and shaded spruce needles, were upscaled to the level of a forest canopy with (i) the DART, and (ii) the PARAS model. In DART the simulated R_L and T_L of the three needle age-classes were averaged per vertical crown level (Fig.1 a-c).

This means that one weighted averaged R_L and T_L spectrum per vertical level (exposed, transitional and shaded level –section II.B) was introduced as input for the canopy BRF simulations. The applied weights were those presented for the same research site by [22] in their Table I. The main biochemical parameter driving different spectral responses between sunlit and shaded needles at our study site was found to be the Cab concentration. An analysis of our needle samples done by [29] showed that shade adapted needles had higher chlorophyll a and b concentrations, which resulted in a slight reflectance and transmittance decrease in visible wavelengths. However, Fig. 1a, c is showing the PROSPECT simulations for the Cab concentration of all simulated cases varying from 10-100 µg cm^{-2}. In addition, the variation found in other biochemical parameters was more pronounced in needles of the 1st year as compared to older generations, rather than between different vertical levels. Thus, the optical properties of sun exposed and shaded needles (Fig. 1a, c) look very similar.

The PARAS model requires a single leaf optical spectrum of the needle-leaf albedo (ω_L), i.e. sum of R_L and T_L. Unlike in DART, where 3D-voxels allow introducing more detailed information in the vertical canopy profile and per individual tree, the ω_L in PARAS represents needles of the whole forest scene. Thus, for PARAS the input R_L and T_L were computed as weighted averages of the nine PROSPECT simulated spectra, with the weights published by [22]. The final ω_L of the stand was calculated as the sum of these weighted averages (Fig. 1d). The use of different parameterizations for both models is an essential part of the objective of this study, which aims to compare the performance of a complex RT model using a very detailed 3D structural forest description (DART) with a model of simpler structural parameterization (PARAS).

D. Top-of-canopy reflectance simulations with DART

Canopy BRF was first simulated by the DART model. Basic parameters of DART simulations are presented in Table II and the structural parameters used for building the detailed DART 3D forest scene are provided in [23] (Table 3). Eight spectral bands corresponding to the red and red-edge bands of the CHRIS-PROBA image (with central wavelengths at 670, 681, 689, 695, 701, 707, 714 and 720 nm) were simulated. All combinations of five LAIs and ten Cab values resulted in 50 BRF simulations of the PROSPECT-DART model per single spectral band. For comparison purposes with PARAS simulations the canopy-cover (CC) of DART forest scenes was fixed at 90%, as measured on average (± 5%) at the study site with LAI-2000. The parameter was approximated as $1-cgf(\theta_1)$ [30], where $cgf(\theta_1)$ is the canopy gap fraction (cgf) in the direction of the viewing zenith angle (θ_1). The output of DART simulations will be referred to as the DART Look-Up-Table.

E. Top-of-canopy reflectance simulations with PARAS

For comparison purposes, the 3D forest description and the sensor and solar angular specifications used to generate the DART Look-Up-Table were also applied to simulate the PARAS Look-Up-Table of BRF values (Table II). In PARAS, the forest BRF is calculated as a sum of the understory and canopy components through the equation

$$BRF = cgf(\theta_1)cgf(\theta_1)\rho_{ground} + f(\theta_1,\theta_2)i_0(\theta_2)\frac{\omega_L - p\omega_L}{1 - p\omega_L}, \quad (1)$$

where θ_1 and θ_2 denote the view (sensor) and solar zenith directions, *cgf* denotes the canopy gap fraction, ρ_{ground} is the BRF of the forest understory, *f* describes the directional distribution of the reflected radiation, i_0 is the canopy interceptance (i.e. fraction of the incoming radiation hitting canopy elements), *p* is the photon recollision probability, and ω_L is the single scattering leaf (needle) albedo.

The *cgf* values extracted from LAI-2000 measurements are the device readings corresponding to the concentric rings whose angles are closest to θ_1 and θ_2, respectively. The ρ_{ground} was expressed as the weighted average from bare soil and senescent needle leaf spectra (section II.B). The *f* function was calculated based on the data provided by [31] (Table 2) as $f = 0.0593LAI+0.5$, which corresponds to a forest stand structure comparable to our study site. The i_0 was computed from the *cgf* as $(1 - cgf(\theta_2))$ and the average *p* was estimated as in [32]:

$$p = 1 - \frac{i_D}{LAI + BAI}, \quad (2)$$

where i_D is the canopy diffuse interceptance approximated as (1-DIFN), i.e. one minus the "diffuse non-interceptance". Stenberg et al. [32] demonstrated that inclusion of the BAI proportion in the photon recollision probability computation of PARAS (2) resulted in forest albedo values that were closer to those simulated by a detailed Forest Radiative Transfer (FRT) model [33]. Canopy LAI was estimated from the effective LAI (LAI_{eff}) measured by LAI-2000 as $LAI = 1.6*LAI_{eff}$. The site-specific coefficient 1.6, derived from field destructive measurements [26], corrects for both the shoot-clumping and the presence of woody biomass. To incorporate the annual variability of LAI into the PARAS Look-Up-Table simulations, we used a normally distributed LAI dataset collected between 2005 and 2007 (section II.B). For comparison purposes, only LAI values matching the values used in DART simulations (i.e. LAI=3-11 in steps of 2, Table II) were used to build the PARAS Look-Up-Table. For each selected LAI the corresponding *cgf* and DIFN recorded by the LAI-2000 were extracted and used in the corresponding equations. The branch area index (BAI) was computed as BAI=0.3*LAI, where 0.3 is a site-specific coefficient derived also from destructive measurements [34]. Including the proportion of woody elements in the calculation of the probability *p* (2) requires computing the ω_L as a weighted average of the albedo from the needle and canopy woody elements [32]. Weights were based on the LAI and the BAI,

respectively, assuming that LAI+BAI=1. The ratio of weights for LAI ($Weight_{LAI}$) and BAI ($Weight_{BAI}$), respectively, was assumed to be the before mentioned 0.3 irrespective of the change in LAI. Finally, PARAS BRF, originally simulated between 450 and 1000 nm with a spectral resolution of 5 nm due to the conifer-adjusted PROSPECT, was resampled to a resolution of 1 nm and subsequently convoluted into the eight CHRIS-PROBA bands according to their spectral response functions.

F. Cab estimation for CHRIS-PROBA data using optical indices

We implemented and cross-compared two Cab retrievals from the CHRIS-PROBA image. The first approach used the chlorophyll sensitive optical index presented by [14] named $ANCB_{650–720}$ that is defined as the Area Under Curve of the continuum-removed (CR) reflectance between 650 and 720 nm ($AUC_{650–720}$) normalized by the CR Band Depth at 670 nm (CBD_{670}). This spectral region was chosen to include the most sensitive Cab absorption wavelengths and to avoid the negative interferences of canopy structure at the longer wavelengths of the red-edge region.

In our study, this wavelength range corresponded to the 4th and 11th CHRIS-PROBA bands, i.e. 670 and 720 nm, defining the index as:

$$ANCB_{670-720} = \frac{AUC_{670-720}}{CBD_{681}}. \quad (3)$$

$AUC_{670–720}$ is computed as:

$$AUC_{670-720} = \frac{1}{2}\sum_{j=1}^{n-1}(\lambda_{j+1} - \lambda_j)(\rho_{j+1} - \rho_j), \quad (4)$$

where ρ_j and ρ_{j+1} are the values of the continuum-removed reflectance at the bands j and j+1, λ_j and λ_{j+1} are the wavelengths of the bands j and j+1, and n is the number of used spectral bands. Broadening the spectral interval towards the 3rd CHRIS-PROBA band at 630 nm would include wavelengths influenced significantly by absorptance of red foliar pigments Anthocyanins [35], which have a negative confounding effect on the performance of the indices for Cab estimation, especially in cases of low Cab values. Since the continuum-removed band depth at 670 nm is for the given wavelength range equal to zero, the next band at 681 nm was selected for the normalization (CBD_{681}). A subsequent sensitivity analysis with the simulated continuum-removed BRF confirmed that this band provides the most stable CBD among the available wavelengths with respect to the systematic Cab variations (results not shown).

The $ANCB_{650-720}$ is a variant of the optical index $ANMB_{650-725}$ defined in [36]. For the latter, the used wavelength range is 650-725 nm and the maximum band depth is used for the normalization (5). Adapting this index to the available CHRIS-PROBA bands resulted into the following definition:

$$ANMB_{670-720} = \frac{AUC_{670-720}}{MBD_{670-720}}, \quad (5)$$

where $MBD_{670-720}$ refers to the maximal band depth of the continuum-removed reflectance between 670 and 720 nm, i.e. one of the spectrally stable and the strongest chlorophyll absorption wavelengths between 681 and 695 nm.

The most appropriate empirical functions describing the behaviour of optical indices in relation to changing Cab were expected to be exponential as published in [14]. The best fitting exponential equations were selected based on the best combination with the highest coefficient of determination R^2, the highest degree-of-freedom adjusted R^2, the lowest fit standard error, and the largest F-test ratio (tested at the probability level $p \leq 0.05$). They were then applied per-pixel to the CHRIS-PROBA image to estimate Cab. The Cab estimates obtained per index and per RT model were cross-compared by computing the root mean square error (RMSE), and the corresponding systematic (RMSEs) and unsystematic RMSE (RMSEu) [37] (Eq. (6), (7) and (8) in [14], respectively).

Finally, Cab CHRIS-PROBA estimates were compared against a Cab map created from an airborne AISA Eagle image of the study area acquired at 0.4 m spatial resolution on September 14th, 2006. Cab was estimated from the AISA image by a conventional artificial neural network (ANN) trained with continuum removed PROSPECT-DART simulated BRF as published in [14]. In order to minimise the negative noise influence and to obtain the most accurate Cab map from the AISA Eagle image, further referred as the ANN AISA dataset, only sunlit pixels of spruce crowns were extracted and analysed the same way as in [14] (see section 2.2). This reference dataset was successfully validated using the laboratory analysed Cab needle-samples collected from ten selected spruce trees [14]. We selected 56 validation polygons of 17 x 17 m^2 (i.e., size of a single CHRIS-PROBA image pixel) located in both the CHRIS and the ANN AISA images. The BRF similarity found between validation polygons extracted from CHRIS-PROBA data and the AISA image used to create the Cab validation map (Fig. 2c, d) suggested sufficient reliability of the AISA reflectance. An average Cab computed per polygon of the ANN AISA retrieval (≈ 1000 AISA sunlit pixels per polygon) was compared to the Cab of the corresponding CHRIS-PROBA pixel. The Cab estimation performance of each optical index per model was assessed using RMSE, RMSEs and RMSEu [37]. The shaded pixels in the ANN-AISA dataset (representing 44% of the validation polygons) were omitted to avoid less accurate Cab estimates caused by: a) an inability of DART to reasonably reproduce shadows due to the simplifications of crown architecture, and b) a high noise of AISA shadowed pixels when the reflectance signal is very low (around 680 nm). In a 17 m x 17 m polygon

we have enough sunlit pixels to produce a representative value when averaged. To test the influence of the shaded pixel omission, we applied the ANCB exponential functions for Cab estimation published by [14], and estimated Cab from: a) only the sunlit crown pixels inside the validation polygons, b) only the shaded ones, and c) both sunlit and shaded. Comparison of all three outputs with the CHRIS-PROBA Cab estimates revealed the lowest standard error and the narrowest confidence interval for the ANN-AISA sunlit dataset. This demonstrates that inclusion of shaded crown pixels increased noise and supports the idea of the sunlit ANN-AISA Cab estimates being a more reliable validation dataset (see results in Table IV).

III. Results And Discussion

A. DART versus PARAS simulated BRF

Fig. 2a presents PARAS and DART simulated BRF of each spectral band averaged over all LAI and Cab input values. The PARAS BRF is systematically higher than the DART BRF. Also the standard deviation (STD) of the PARAS simulated BRF (0.05-0.06) is higher than the STD of the DART simulated BRF (0.02), which is caused by a higher sensitivity of PARAS BRF simulations to the specified LAI values (Fig. 2a). PARAS BRF is systematically higher than the DART BRF for LAI < 5, while for LAI ≥ 7 the deviation between models decreases (Fig. 2b). The cross-comparison between PARAS and DART BRF values shows a non-linear relationship (R^2= 0.56) with an RMSE equal to 0.04, where RMSEs > RMSEu indicates that the deviation is not random. However, when cross-comparing BRF per LAI a linear relationship appears for all cases (R^2=0.99). This suggests that canopy RT modelling of both models is comparable for LAI ≥ 7, where a nearly 1:1 relationship between BRF of both models resulted in RMSEs ≤ 0.01 (RMSEu=0). If LAI < 7, then the RMSE increases (RMSE=0.05-0.08).

A first possible cause of the systematic discrepancy observed between the BRF simulations in Fig. 2 is the different parameterisation of the input leaf optical properties in PARAS and DART as described in section II.C. Secondly, the ratio of $Weight_{LAI}$ and $Weight_{BAI}$ is in PARAS defined as constant irrespective of the LAI change (section II.E). As expected, BRF simulated by PARAS for LAI values closer to the true LAI of the study site in 2006, i.e. LAI=7 and 9, are approaching the CHRIS-PROBA and AISA observed reflectance (Fig. 2c, d). However, with decreasing LAI and higher spectral contribution from woody parts to BAI, the ratio of $Weight_{BAI}$ and $Weight_{LAI}$ is not constant, which is biasing ω_L for cases of low LAI, and consequently affecting simulated BRF. Further analyses on how these weights are affecting the simulated BRF would help to assess the importance of this discrepancy. However, they are outside the scope of this paper.

B. Empirical relationships between Cab and optical indices based on DART and PARAS simulations

The Cab sensitive optical indices $ANCB_{670\text{-}720}$ and $ANMB_{670\text{-}720}$ were computed from the DART and PARAS simulated Look-Up-Tables and related to the Cab model input. The exponential functions corresponding to the best fit between Cab and the simulated indices are listed in Table III and plotted in Fig. 3. Although the functions are expressing the overall relationships as simulated by the two models, the index values are plotted per LAI to demonstrate how LAI affects the fitting (Fig. 3).

Results show a lower sensitivity of $ANMB_{670\text{-}720}$ to LAI variation than $ANCB_{670\text{-}720}$ for both models. On the one hand, the DART and PARAS based $ANMB_{670\text{-}720}$ shows very little confounding effects of LAI (Fig. 3b and d) resulting in strong and stable Cab-$ANMB_{670\text{-}720}$ relationships (R^2=0.99 and R^2=0.95, respectively). On the other hand, the PARAS based $ANCB_{670\text{-}720}$ index (Fig. 3c) is strongly affected by the LAI, which resulted in a poor curve fitting result (R^2=0.65). However, for its DART counterpart the statistical relationship with Cab is considerably better (R^2=0.97), despite a small dispersion of $ANCB_{670\text{-}720}$ due to the LAI with Cab ≥ 50 µg cm^{-2} (Fig. 3a). The differences in performance of both indices generated by the same model are caused by their mathematical definition. Specifically, the area under the continuum-removed BRF curve ($AUC_{670\text{-}720}$) is in the case of $ANCB_{670\text{-}720}$ normalized to the continuum-removed BRF at the wavelength of 681 nm (CBD_{681}, (3)), while in the case of $ANMB_{670\text{-}720}$ it is normalized to the continuum-removed BRF at the maximum band depth of the whole range 670-720 nm ($MBD_{670\text{-}720}$, (5)). Although both indices were designed to be LAI insensitive [14, 36], our analysis showed that the normalization effect by CBD_{681} is in case of PARAS simulated $ANCB_{670\text{-}720}$ (Fig 3c) disturbed, most likely by a model parameterization insufficiency.

C. Cab estimated from CHRIS-PROBA data

In all cases, the Cab values, which were retrieved from the CHRIS-PROBA image (176 image pixels) using equations presented in Table III, varied within the Cab ranges published previously for the study site in [14, 28]. Since the laboratory Cab extractions from collected needle samples provided validation ground truth only for Cab estimation of single tree crowns, they could not be used to assess the accuracy of the CHRIS-PROBA Cab estimates representing canopies of several trees. To indirectly validate the per-pixel CHRIS-PROBA Cab estimates, we, therefore, cross-compared their values with the Cab map produced by an ANN from the airborne AISA image of the study area. Fig. 4 and Fig. 5 show the results of $ANCB_{670\text{–}720}$ and $ANMB_{670\text{–}720}$ estimates, respectively, for both RT models. Fig. 4a and 5a indicate a strong linear relationship between DART and PARAS estimated Cab. The $ANCB_{670\text{–}720}$ results reveal a smaller overall difference between DART and PARAS based Cab estimates (RMSE=5.8 µg cm^{-2}) than the $ANMB_{670\text{–}720}$ results (RMSE=17 µg cm^{-2}). In both cases the error is, as expected, prevailingly systematic (RMSEs>RMSEu). The slope of the

linear function is steeper for the $ANCB_{670–720}$ case, resulting in an increasing deviation between the two model results with increasing Cab. In case of the $ANMB_{670–720}$, a nearly 1:1 linear relationship with a systematic offset of 11 μg cm^{-2} of DART Cab estimates with respect to PARAS ones was found. The linear relationships signalize similar, but systematically biased performance of both RT models, resulting in higher Cab estimates for DART. As explained in section III.A, the probable reason for higher DART estimates is the difference in weighting of the input R_L and T_L spectra (section II.C). Thus, a seemingly small anomaly in parameterization of the PROSPECT model, especially in the upper vertical crown levels of the DART simulated forest scene, may potentially result in the systematic offset observed in Fig. 5.

D. Validation CHRIS-PROBA derived Cab estimates

To validate CHRIS-PROBA Cab estimates at spatial resolution of 17 m we used the ANN-AISA Cab map, which is a product derived from very high spatial resolution airborne AISA data (pixel size of 0.4 m) based on an upscaling radiative transfer retrieval approach.

Subplots (b) and (c) in Fig. 4 and Fig. 5 show how Cab values extracted with the two indices compare with the reference Cab map estimated from AISA data using ANN [14]. The Cab estimates in Fig. 4 based on PARAS are quantitatively closer to the airborne Cab map than the Cab values based on DART (RMSE = 2.7 μg cm^{-2} and 7.5 μg cm^{-2}, respectively). The RMSE for DART is dominated by the systematic error (RMSEs), which indicates that a systematic change in DART modelling approach could improve the performance of the $ANCB_{670–720}$ retrieval procedure. Validation of the ANMB–counterpart (Fig. 5b and c) showed that the Cab point clouds are similar, with DART results being higher by an offset of 11 μg cm^{-2}, resulting in a lower RMSE for PARAS (RMSE = 9.5 μg cm^{-2}) than for DART (RMSE = 23 μg cm^{-2}). For both models, the same poor relationships with the ANN-AISA Cab occurred, with the RMSEs dominating the RMSE. This suggests that although $ANMB_{670–720}$ demonstrates closer and LAI independent relations with simulated Cab classes (Fig. 3), it does not necessarily produce more accurate estimates than $ANCB_{670–720}$. Moreover, results of section III.B showed that the Cab estimating function based on $ANCB_{670-720}$ simulated by PARAS is highly sensitive to LAI and the least reliable retrieval equation out of the four presented in Fig 3. When comparing the average Cab estimates (i.e., mean of all validation pixels) resulting from different approaches (TABLE IV), Cab estimated through the DART $ANMB_{670–720}$ approach showed the highest dispersion (i.e., standard deviation), the highest standard error, and the widest 95% confidence interval (i.e. range of values that includes the true value of the population with a 95% probability) indicating high uncertainty around the estimate. This result is attributed to the detailed DART parameterization of needle spectra R_L and T_L, which requires further analyses. Finally, the results are specific for the functional type of canopy analysed in this study. Further investigation is therefore needed to evaluate the performance of both RT models for more biologically diverse and structurally complex forest stands.

IV. CONCLUSION

This study demonstrates that needle-leaf Cab retrieved with a leaf-canopy radiative transfer model based on the photon-recollision probability (PARAS), using the continuum-removed reflectance of red and red-edge wavelengths (670–720 nm) acquired by the space borne CHRIS-PROBA spectroradiometer, can lead to results comparable with a complex 3D radiative transfer model (DART). This suggests that, despite less input parameters and its simplicity, PARAS presents an alternative to more detailed and complex 3D radiative transfer canopy models when applied to satellite imaging spectroscopy data with a spatial resolution of tens of meters. The Cab values retrieved from the CHRIS PROBA imaging spectroscopy image using the PARAS-$ANMB_{670-720}$ algorithm were systematically lower than the estimates produced by the DART-$ANMB_{670-720}$ approach, following a nearly one-to-one relationship with an offset of 11 μg cm^{-2}. Such a strong linear relationship implies that the RT modelling of both canopy models is comparable; the obtained systematic offset is most probably caused by differences in model parameterizations. Further analysis on the impact of the optical parameterization of needles and woody elements may, therefore, reduce this BRF bias. The Cab estimates of both models produced by the $ANCB_{670-720}$ index were also linearly related, but the difference was systematically increasing with increasing Cab.

Modelling results revealed that the PARAS simulated BRF is more sensitive to the predefined LAI parameters than the BRF simulated with DART. Although empirical relationships between Cab and the indices were more robust for DART due to this sensitivity, Cab estimations of both indices based on the PARAS model were closer to the Cab values extracted from an AISA image using an artificial neural network inversion approach. Interestingly, the $ANCB_{670-720}$ approach for both models yielded lower RMSE values computed between the CHRIS-PROBA and the airborne Cab estimates, even though the empirical functions fitted using $ANCB_{670-720}$ were statistically less robust than for $ANMB_{670-720}$.

ACKNOWLEDGMENT

The authors thank Dr. Radek Pokorný and Dr. Lucie Homolová from the Academy of Sciences of the Czech Republic for acquisition and processing of PCA LAI-2000 data and Prof. Jean-Philippe Gastellu-Etchegorry from the CESBIO Laboratory (France) for providing the DART model that allowed us to conduct this study.

REFERENCES

[1] M. Chen, M. Schliep, R. D. Willows, Z. L. Cai, B. A. Neilan, and H. Scheer, "A red-shifted chlorophyll," *Science*, vol. 329, pp. 1318-1319, 2010.

[2] G. A. Blackburn, "Hyperspectral remote sensing of plant pigments," *Journal of Experimental Botany*, vol. 58, pp. 855-867, 2007.
[3] S. L. Ustin, A. A. Gitelson, S. Jacquemoud, M. Schaepman, G. P. Asner, J. A. Gamon, and P. Zarco-Tejada, "Retrieval of foliar information about plant pigment systems from high resolution spectroscopy," *Remote Sensing of Environment*, vol. 113, pp. S67-S77, 2009.
[4] G. le Maire, C. François, K. Soudani, D. Berveiller, J. Y. Pontailler, N. Bréda, H. Genet, H. Davi, and E. Dufrêne, "Calibration and validation of hyperspectral indices for the estimation of broadleaved forest leaf chlorophyll content, leaf mass per area, leaf area index and leaf canopy biomass," *Remote Sensing of Environment*, vol. 112, pp. 3846-3864, 2008.
[5] J. L. Widlowski, M. Taberner, B. Pinty, V. Bruniquel-Pinel, M. Disney, R. Fernandes, J. P. Gastellu-Etchegorry, N. Gobron, A. Kuusk, T. Lavergne, S. Leblanc, P. E. Lewis, E. Martin, M. Mõttus, P. R. J. North, W. Qin, M. Robustelli, N. Rochdi, R. Ruiloba, C. Soler, R. Thompson, W. Verhoef, M. M. Verstraete, and D. Xie, "Third Radiation Transfer Model Intercomparison (RAMI) exercise: Documenting progress in canopy reflectance models," *Journal of Geophysical Research D: Atmospheres*, vol. 112, 2007.
[6] J. Verrelst, M. E. Schaepman, B. Koetz, and M. Kneubühler, "Angular sensitivity analysis of vegetation indices derived from CHRIS/PROBA data," *Remote Sensing of Environment*, vol. 112, pp. 2341-2353, 2008.
[7] J. M. Chen, "Optically-based methods for measuring seasonal variation of leaf area index in boreal conifer stands," *Agricultural and Forest Meteorology*, vol. 80, pp. 135-163, 1996.
[8] P. Stenberg, "Correcting LAI-2000 estimates for the clumping of needles in shoots of conifers," *Agricultural and Forest Meteorology*, vol. 79, pp. 1-8, 1996.
[9] P. Stenberg, "A note on the G-function for needle leaf canopies," *Agricultural and Forest Meteorology*, vol. 136, pp. 76-79, 2006.
[10] T. Nilson, "Inversion of gap frequency data in forest stands," *Agricultural and Forest Meteorology*, vol. 98-99, pp. 437-448, 1999.
[11] M. Rautiainen and P. Stenberg, "Application of photon recollision probability in coniferous canopy reflectance simulations," *Remote Sensing of Environment*, vol. 96, pp. 98-107, 2005.
[12] S. G. Leblanc, P. Bicheron, J. M. Chen, M. Leroy, and J. Cihlar, "Investigation of directional reflectance in boreal forests with an improved four-scale model and airborne POLDER data," *Geoscience and Remote Sensing*, IEEE Transactions on, vol. 37, pp. 1396-1414, 1999.
[13] J. P. Gastellu-Etchegorry, E. Martin, and F. Gascon, "DART: A 3D model for simulating satellite images and studying surface radiation budget," *International Journal of Remote Sensing*, vol. 25, pp. 73-96, 2004.
[14] Z. Malenovský, L. Homolová, R. Zurita-Milla, P. Lukeš, V. Kaplan, J. Hanuš, J. P. Gastellu-Etchegorry, and M. E. Schaepman, "Retrieval of spruce leaf chlorophyll content from airborne image data using continuum removal and radiative transfer," *Remote Sensing of Environment*, vol. 131, pp. 85-102, 2013.
[15] R. Hernández-Clemente, R. M. Navarro-Cerrillo, and P. J. Zarco-Tejada, "Carotenoid content estimation in a heterogeneous conifer forest using narrow-band indices and PROSPECT+DART simulations," *Remote Sensing of Environment*, vol. 127, pp. 298-315, 2012.
[16] P. Stenberg, M. Mõttus, and M. Rautiainen, "Modeling the Spectral Signature of Forests: Application of Remote Sensing Models to Coniferous Canopies," in *Advances in Land Remote Sensing*, S. Liang, Ed.: Springer Netherlands, 2008, pp. 147-171.
[17] G. Schaepman-Strub, M. E. Schaepman, T. H. Painter, S. Dangel, and J. V. Martonchik, "Reflectance quantities in optical remote sensing-definitions and case studies," *Remote Sensing of Environment*, vol. 103, pp. 27-42, 2006.
[18] S. Smolander and P. Stenberg, "A method to account for shoot scale clumping in coniferous canopy reflectance models," *Remote Sensing of Environment*, vol. 88, pp. 363-373, 2003.
[19] [19] M. Rautiainen, J. Suomalainen, M. Mõttus, P. Stenberg, P. Voipio, J. Peltoniemi, and T. Manninen, "Coupling forest canopy and understory reflectance in the Arctic latitudes of Finland," *Remote Sensing of Environment*, vol. 110, pp. 332-343, 2007.
[20] J. Heiskanen, M. Rautiainen, L. Korhonen, M. Mõttus, and P. Stenberg, "Retrieval of boreal forest LAI using a forest reflectance model and empirical regressions," *International Journal of Applied Earth Observation and Geoinformation*, vol. 13, pp. 595-606, 2011.
[21] M. A. Cutter, D. R. Lobb, and R. A. Cockshott, "Compact High Resolution Imaging Spectrometer (CHRIS)," *Acta Astronautica*, vol. 46, pp. 263-268, 2000.
[22] P. Lukeš, M. Rautiainen, P. Stenberg, and Z. Malenovský, "Empirical test of the spectral invariants theory using imaging spectroscopy data from a coniferous forest," *International Journal of Applied Earth Observation and Geoinformation*, vol. 13, pp. 668-675, 2011.
[23] Z. Malenovský, E. Martin, L. Homolová, J. P. Gastellu-Etchegorry, R. Zurita-Milla, M. E. Schaepman, R. Pokorný, J. G. P. W. Clevers, and P. Cudlín, "Influence of woody elements of a Norway spruce canopy on nadir reflectance simulated by the DART model at very high spatial resolution," *Remote Sensing of Environment*, vol. 112, pp. 1-18, 2008.
[24] R. Pokorný, I. Tomáškova, and K. Havrankova, "Temporal variation and efficiency of leaf area index in young mountain Norway spruce stand," *European Journal of Forest Research*, vol. 127, pp. 359-367, 2008.
[25] L. Homolová, Z. Malenovský, J. Hanuš, I. Tomášková, M. Dvořáková, and R. Pokorný, "Comparison of different ground techniques to map leaf area index of Norway spruce forest canopy," in *Proceedings 10th International Symposium on Physical Measurements and Spectral Signatures in Remote Sensing* (ISPMSRS), Davos, Switzerland, 2007, pp. 499 - 504.
[26] R. Pokorný and M. V. Marek, "Test of accuracy of LAI estimation by LAI-2000 under artificially changed leaf to wood area proportions," *Biologia Plantarum*, vol. 43, pp. 537-544, 2000.
[27] S. Jacquemoud and F. Baret, "PROSPECT: A model of leaf optical properties spectra," *Remote Sensing of Environment*, vol. 34, pp. 75-91, 1990.
[28] Z. Malenovský, J. Albrechtová, Z. Lhotáková, R. Zurita-Milla, J. G. P. W. Clevers, M. E. Schaepman, and P. Cudlín, "Applicability of the PROSPECT model for Norway spruce needles," *International Journal of Remote Sensing*, vol. 27, pp. 5315-5340, 2006.
[29] L. Homolova, Z. Malenovský, Z. Lhotáková, V. Kaplan, and J. Hanuš, "Optical differences between sun exposed and shaded Norway spruce needles " in *Proceedings 5th EARSeL Workshop on Imaging Spectroscopy*, Bruges, Belgium, 2007.
[30] M. Rautiainen, P. Stenberg, and T. Nilson, "Estimating canopy cover in scots pine stands," *Silva Fennica*, vol. 39, pp. 137-142, 2005.
[31] M. Mõttus and P. Stenberg, "A simple parameterization of canopy reflectance using photon recollision probability," *Remote Sensing of Environment*, vol. 112, pp. 1545-1551, 2008.
[32] P. Stenberg, Lukeš, P., M. Rautiainen, and T. Manninen, "A new approach for simulating forest albedo based on spectral invariants," *Remote Sensing of Environment*, vol. 137, pp. 12-16, 2013.
[33] A. Kuusk and T. Nilson, "A directional multispectral forest reflectance model," *Remote Sensing of Environment*, vol. 72, pp. 244-252, 2000.
[34] R. Pokorný and I. Tomáškova, "Allometric relationships for surface area and dry mass of young Norway spruce aboveground organs," *Journal of Forest Science*, vol. 53, pp. 548–554, 2007.
[35] M. N. Merzlyak, T. B. MelÃ¸, and K. Razi Naqvi, "Estimation of leaf transmittance in the near infrared region through reflectance measurements," *Journal of Photochemistry and Photobiology B: Biology*, vol. 74, pp. 145-150, 2004.
[36] Z. Malenovský, C. M. Ufer, J. G. P. W. Clevers, M. E. Schaepman, J. Albrechtová, and P. Cudlín, "A new hyperspectral index for chlorophyll estimation of a forest canopy: Area under curve Normalized to Maximal Band depth between 650-725 nm," *EARSeL eProceedings 5*, pp. 161-172, 2006.
[37] C. J. Willmott, "On the validation of models," *Physical Geography*, vol. 2, pp. 184-194, 1981.

Lucia Yáñez-Rausell received the degree in forestry engineering from the Universidad Politecnica of Madrid, Spain, in 2005 and the M.Sc. degree in geo-information science from Wageningen University, The Netherlands, in 2006. In 2007 she worked as research assistant at CSIRO Land and Water, in Canberra, ACT, Australia. She is currently working toward the Ph.D. degree in the Laboratory of Geo-information Science and Remote Sensing at Wageningen University and working at the Department of Geography, Remote Sensing Laboratories, University of Zurich, Switzerland. Her recent interests include remote sensing of

bio- and geophysical parameters for vegetation monitoring studies using radiative transfer models and imaging spectroscopy.

Zbyněk Malenovský (M'06) received the M.Sc. degree in terrestrial ecology from the Palacký University, Olomouc, Czech Republic, in 1998, and the Ph.D. degree in production ecology and resource conservation from Wageningen University, The Netherlands, in 2006. He was previously with Remote Sensing Laboratories at University of Zurich, Switzerland. Since 2012 he has been a Research Associate at University of Tasmania and at University of Wollongong in Australia. In his main research interest belong optical remote sensing approaches assessing quantitatively stress-related physiological characteristics of vegetation using the models of radiative transfer at both leaf and canopy scales.

Miina Rautiainen received the M.Sc. degree in biology from the University of Turku, Turku, Finland, in 2002, and the Ph.D. degree (with distinction) in forest science from the University of Helsinki, Helsinki, Finland in 2005.

She is currently an Academy of Finland Research Fellow in the Department of Forest Sciences at the University of Helsinki. Her current research interests include the development and application of forest reflectance models and remote sensing of forest structure.

Jan G. P. W. Clevers received the M.Sc. degree in agronomy and the Ph.D. degree in remote sensing from Wageningen University, Wageningen, The Netherlands, in 1981 and 1986, respectively. His current research interests include the continuation of the developments of optical reflectance models (including bidirectional reflectance and hyperspectral measurements), the linking to crop growth models, the synergy hypothesis with the purpose of the combined use of optical and microwave observations as well as of prior knowledge, and land cover mapping using remote sensing data at different scales. He is currently an Associate Professor and Lecturer in remote sensing at Wageningen University.

Petr Lukeš received a B.S. and M.S. degrees in geoinformatics from the Technical University of Ostrava, in 2007 and the Ph.D. degree in geoinformatics from Mendel University Brno in 2012. From 2007 to 2011, he was a Research Assistant with the Global Change Research Centre AS CR. Since 2012, he is a post-doctoral researcher with Department of Forest Sciences at the University of Helsinki. His research interests include remote sensing of vegetation, radiative transfer modelling in forest canopies, imaging spectroscopy and optical properties of leaves.

Jan Hanuš received an M.Sc. degree in geodesy from the Czech Technical University, Prague, in 2002. He is employed as researcher at CVGZ AV ČR - CzechGlobe since 2005. His main research interests are in spectroscopy, imaging spectroscopy and corrections (atmospheric, radiometric, geometric) of hyperspectral data.

Michael E. Schaepman (M'05–SM'07) received the M.Sc. degree and the Ph.D. degree in geography from the University of Zurich (UZH), Zurich, Switzerland, in 1993 and 1998, respectively.

In 1999, he spent his postdoctoral time at the Optical Sciences Center, The University of Arizona, Tucson. In 2000, he was appointed Project Manager of the European Space Agency Airborne Prism Experiment spectrometer. In 2003, he accepted the position of Full Chair of geoinformation science and remote sensing at Wageningen University, Wageningen, The Netherlands. In 2009, he was appointed Full Chair of remote sensing at UZH, where he is currently heading the Remote Sensing Laboratories, Department of Geography. His interests are in computational Earth sciences using remote sensing and physical models, with particular focus on the land–atmosphere interface using imaging spectroscopy.

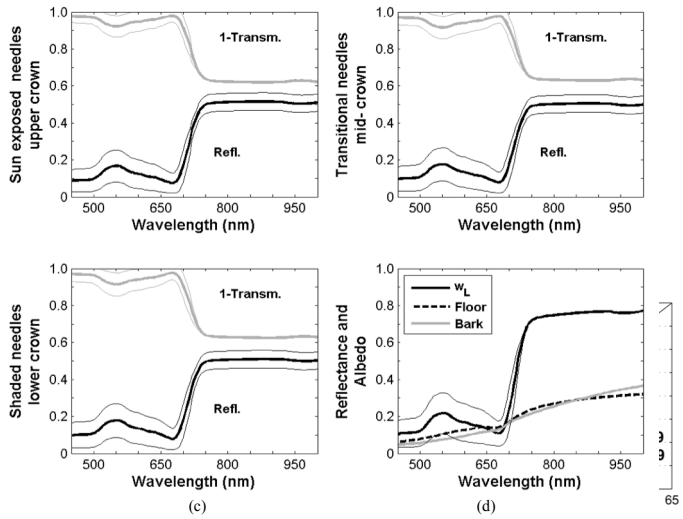

Fig. 1. Spectral inputs used for both DART and PARAS model simulations: (a-c) Average needle-leaf reflectance and transmittance (plotted as 1-Transm.) simulated with the PROSPECT leaf RT model (version 3) [27], adjusted for Norway spruce needles by [28]. Spectra are averaged for the three needle age-classes per vertical crown profile: sun exposed (a), transitional (b) and shaded (c) (Average=thicker lines; ±standard-deviation=thinner lines), and (d) needle-leaf albedo computed as weighted average of the nine PROSPECT simulated spectra used as input for PARAS model (ω_L), bark reflectance ("Bark") and understory reflectance ('Floor'). The weights applied here were those presented for the same research site by [22].

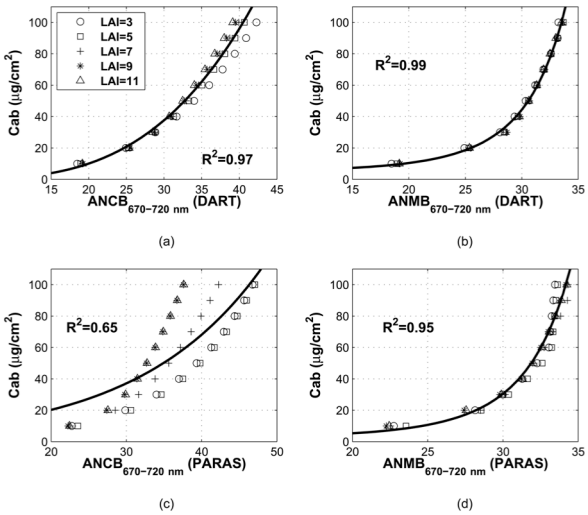

Fig. 3. Relationship between Cab and respectively $ANCB_{670-720}$ (a and c) and $ANMB_{670-720}$ (b and d) computed from DART simulated BRF (a and b) and PARAS simulated BRF (c and d) for the LAI range 3-11 m^2m^{-2} in steps of 2 m^2m^{-2}. Index values corresponding to each LAI are represented by different symbols.

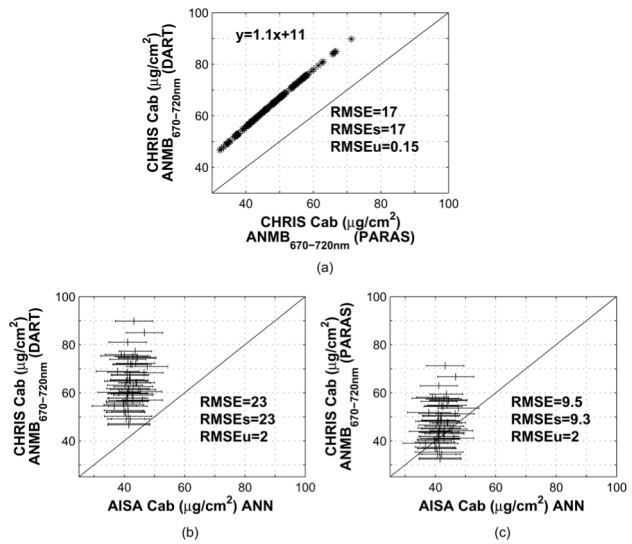

Fig. 5. Same figure as Fig. 4, with results corresponding to the $ANMB_{670-720}$.

simulated spectral band, (b) comparison between PARAS BRF and DART BRF per LAI (R^2 is the coefficient of determination of the overall linear function; RMSE is the root-mean squared error; RMSEs is the systematic RMSE; and RMSEu is the unsystematic RMSE computed according to Eq. (6), (7) and (8) in [14], respectively), (c) PARAS and DART BRF for LAI=7 and observed reflectance extracted from CHRIS-PROBA and AISA validation polygons, and (d) the same as in c) with PARAS and DART BRF for LAI=9.

TABLE I
FIXED AND VARYING INPUT PARAMETERS FOR THE PROSPECT MODEL SIMULATIONS OF NORWAY SPRUCE NEEDLE OPTICAL PROPERTIES

Needle type	Cw (StDev) [cm] n=9	Cm (StDev) [g cm^{-2}] n=9	N (StDev) n=81	Cab [μ cm^{-2}]
Exposed C	0.0221 (0.0054)	0.0177 (0.0046)	2.13 (0.061)	10-100 in steps of 10
Exposed C+	0.0250 (0.0021)	0.0197 (0.0022)		
Exposed C++	0.0246 (0.0042)	0.0202 (0.0028)		
Transitional C	0.0213 (0.0028)	0.0128 (0.0019)		
Transitional C+	0.0230 (0.0039)	0.0157 (0.0023)		
Transitional C++	0.0229 (0.0018)	0.0166 (0.0016)		
Shaded C	0.0169 (0.0027)	0.0102 (0.0026)		
Shaded C+	0.0199 (0.0042)	0.0119 0.0024)		
Shaded C++	0.0234 (0.0046)	0.0149 (0.0024)		

Cw = needle-leaf water column; Cm = needle-leaf mass per area; N = needle-leaf mesophyll structural parameter; C = needles of current growing season; C+ = one year-old needles; C++ = two years-old needles; StDev = standard deviation; n = number of input samples.

TABLE III
EMPIRICAL FUNCTIONS DESCRIBING THE RELATIONSHIP BETWEEN SIMULATED CAB AND OPTICAL INDICES

Index	Fitted Equation	R^2 [a]	Adj R^2 [b]	Fit SE	F-ratio
ANCB (DART)	$y = e^{-7.4505211+3.2571664\ln(x)}$	0.968	0.966	5.27	1438.30
ANMB (DART)	$y = e^{1.7307696+0.000076322471x\wedge 3}$	0.995	0.994	2.15	8911.02
ANCB (PARAS)	$y = 6.0004141e^{0.060745331x}$	0.646	0.631	17.43	87.74
ANMB (PARAS)	$y = e^{0.93134314+0.000091989141x\wedge 3}$	0.952	0.950	6.43	950.43

[a]Coefficient of determination of the function; [b]Degree-of-freedom adjusted coefficient of determination; FitSE = Standard error of the function; F-ratio = the F-test ratio, tested at the probability level $P \leq 0.05$; ANCB = $ANCB_{670\text{-}720;}$; ANMB = $ANMB_{670\text{-}720.}$

TABLE II
FIXED AND VARYING KEY INPUT PARAMETERS FOR DART AND PARAS BRF SIMULATIONS OF A NORWAY SPRUCE SCENE

Parameters common to DART and PARAS models			
Sun position (fixed)	/Real solar noon/		
Zenith angle	θ_s	[°]	46.6
Azimuth angle	ϕ_s	[°]	180
Needle-leaf area Index	LAI	[m^2 m^{-2}]	3-11 in steps of 2 [a]
Simulated CHRIS-PROBA bands (central wavelengths)	λ	[nm]	670, 681, 689, 695, 701, 707, 714 and 720 [b]
Parameters that are specific for DART model			
Slope (fixed)		[°]	13.5
Canopy closure (fixed)	CC	[%]	90

[a]In the PARAS model, field-based LAI values were averaged to match DART simulated LAI ranges; [b]PARAS BRF simulated between 450 and 1000 nm was resampled from 5 to 1 nm spectral resolution and then integrated into the eight CHRIS-PROBA bands.

TABLE IV
MEAN CAB (ALL VALIDATION PIXELS) ESTIMATED PER APPROACH

Dataset	Cab mean	Cab SD	Cab SE	95CI	
ANCB DART CHRIS-PROBA	48	5	0.70	49.1	46.4
ANCB PARAS CHRIS-PROBA	43	3	0.37	43.4	41.9
ANMB DART CHRIS-PROBA	63	9	1.22	65.2	60.4
ANMB PARAS CHRIS-PROBA	46	8	1.08	48.6	44.3
ANN AISA sunlit	42	7	0.03	42.0	41.9
ANCB AISA sunlit	83	11	0.05	83.2	83.0
ANCB AISA shaded	96	30	0.16	97.0	96.2
ANCB AISA sunlit & shaded	89	22	0.07	88.7	88.4

SD = standard deviation; SE = standard error from the mean; 95CI = 95% Confidence interval; ANCB = $ANCB_{670\text{-}720}$; ANMB = $ANMB_{670\text{-}720.}$